Research Article | Vol. 28, No. 19 / 14 September 2020 / Optics Express 28352
Optics EXPRESS

Surface plasticizing of chalcogenide glasses: a route for direct nanoimprint with multifunctional antireflective and highly hydrophobic structures

SIVAN TZADKA,[1,2] NATALI OSTROVSKY,[1,2] ESTI TOLEDO,[1,2] GUILLAUME LE SAUX,[1,2] EVYATAR KASSIS,[3] SHAY JOSEPH,[3] AND MARK SCHVARTZMAN[1,2]

[1] *Deparment of Materials Engineering, Ben-Gurion University of the Negev, Beer-Sheva, Israel*
[2] *Ilse Katz Institute for Nanoscale Science and Technology, Ben-Gurion University of the Negev, Beer-Sheva, Israel*
[3] *Optical Component Center, Rafael Advanced Defense Systems, Haifa, Israel*

Abstract: Chalcogenide glasses are attractive materials for optical applications. However, these applications often require pattering of the surface with functional micro-/ nanostructures, which is challenging by traditional microfabrication. Here, we present a novel, robust, and scalable approach for the direct patterning of chalcogenide glasses, based on soft imprinting of a solvent-plasticized glass layer formed on the glass surface. We established a methodology for surfaces plasticizing, through tuning of its glass transition temperature by process conditions, without compromising on the chemical composition, structure, and optical properties of the plasticized layer. This control over the glass transition temperature allowed to imprint the surface of chalcogenide glass with features sized down to 20 nm, and achieve an unprecedented combination of full pattern transfer and complete maintenance of the shape of the imprinted substrate. We demonstrated two applications of our patterning approach: a diffraction grating, and a multifunctional pattern with both antireflective and highly hydrophobic water-repellent functionalities – a combination that has never been demonstrated for chalcogenide glasses. This work opens a new route for the nanofabrication of optical devices based on chalcogenide glasses and paves the way to numerous future applications for these important optical materials.

1. Introduction

Chalcogenide glasses are attractive materials for infrared optical applications, due to their high transmittance and refractive index, which can be tuned by varying the glass composition [1–3]. Furthermore, their pronounced 3rd order non-linearity makes them appealing for all-optical switching devices [4], and the photon-induced transition between their amorphous and crystalline phases makes hold promise for memory devices and tunable photonics [5,6]. Still, the realization of optical devices based on chalcogenide glasses is often technologically challenging. For instance, many devices employ sub-wavelength light-manipulating structures, such as diffraction gratings or waveguides, whose realization requires fabrication approaches different from those applicable to common optical materials such as silicon-based glasses. Also, chalcogenide glasses naturally reflect up to 30% of mid-infrared light. Thus, high-end optical components made of this material usually require an antireflective coating. Traditional thin-film-based antireflective coatings are based on expensive vacuum deposition technology. Furthermore, the choice of materials for antireflective thin films that are compatible with chalcogenide glasses in terms of refractive index, as well as in terms of adhesion and thermo-mechanics, is very limited [7–9]. An emerging alternative to thin-film based antireflective coating is sub-wavelength micro-/nano-structures bioinspired from the cornea of nocturnal moth *Spodoptera eridania* [10]. These structures produce a highly omnidirectional and broadband antireflective effect [11]. Furthermore, they also

#400038 https://doi.org/10.1364/OE.400038
Journal © 2020 Received 16 Jun 2020; revised 11 Aug 2020; accepted 12 Aug 2020; published 9 Sep 2020

Optics EXPRESS

provide a surface with high hydrophobicity and water-repellent properties referred to as the "lotus leaf effect" [12,13]. These antireflective and self-cleaning micro-/nano-structures have been successfully demonstrated on commonly used optical materials, such as silicon or glass [14,15]. However, the realization of moth-eye structures on chalcogenide glasses is still challenging, as it requires their direct surface patterning in a facile, scalable, and high-throughput manner.

The surface of chalcogenide glasses can be directly patterned by electron beam or laser writing [16–18], however, those are serial, and therefore low-throughput patterning methods that are unsuitable for scalable fabrication. Alternatively, chalcogenide glasses can be thermally imprinted with a soft elastomeric stamp, due to their relatively low glass transition point (T_g), which ranges between 170-185°C for glasses with a two-dimensional network [19]. However, soft imprinting has so far only been demonstrated mostly on thin films of chalcogenide glasses, which were deposited on solid substrates such as silicon [20–23]. On the other hand, a direct surface imprint of bulk chalcogenide glasses has still been fundamentally challenging: applying high imprint pressure and temperature would necessarily deform the imprinted substrate, whereas imprinting with reduced pressure and temperature would result in incomplete pattern transfer [24]. Recent attempts to circumvent this fundamental challenge were based on tightly confining the imprinted substrate within a metallic fixture that should prevent substrate deformation, yet such a fixture should be custom-made for each imprinted substrate [25–27]. Recently, our group demonstrated the radiative nanoimprint of chalcogenide glasses, in which only the interface between the glass and light absorbing mold was heated above the T_g of the imprinted glass, while its bulk stayed below T_g and was thus not deformed [28]. Yet, this approach requires a tight control of the imprint temperature, as well as the complicated fabrication of a light absorbing mold made of a silicone elastomer reinforced with carbon nanotubes. A robust and scalable direct surface pattering of chalcogenide glasses remains a challenge, thus preventing many applications of these promising optical materials.

In this paper, we demonstrate a novel and robust, approach for the direct surface patterning of chalcogenide glasses with functional micro-/nano- structures. As mentioned above, at the crux of the direct imprint is the ability to achieve full transfer pattern on the one hand, while at the same time to maintain the shape of the imprinted substrate on the other hand. To satisfy these two contradictory requirements, we plasticized the surface of chalcogenide glass, by applying onto it a thin layer of the same chalcogenide glass which had been previously solubilized in an organic solvent, then spin-coated and, finally, controllably annealed (Fig. 1(a)). We hypothesized that the residual solvent plasticizes the obtained surface layer, i.e. lowers its T_g compared to the underlying bulk substrate made of pristine chalcogenide glass. We further hypothesized, that the solvent content, and thereby the T_g of the surface layer, can be set by annealing conditions. Thus, a surface imprint at a temperature between the surface T_g and bulk T_g would ensure full pattern transfer, and at the same time prevent substrate deformation.

To verify our hypothesis and the feasibility of our imprint process, we plasticized As_2Se_3 – a chalcogenide glass commonly used in infrared optics. We first systematically studied the impact of the annealing conditions of the T_g of As_2Se surface layer formed from solution and found that it can be controllably lowered by almost 40°C when compared to that of bulk chalcogenide glass, without any substantial change in the glass structure, composition, and optical properties. By a serial of chemical analyses, we found that the controlled reduction of T_g scales with the amount of residual solvent, and concluded that the solvent functions a plasticizing agent that facilitates the thermoforming of the glass, similarly to commercial plasticizers in organic polymers. We harnessed this controlled plasticizing for the surface imprint of As_2Se with nanoscale features sized down to 20 nm and applied this novel imprint approach to the fabrication of several functional microstructures including diffraction gratings and moth-eye antireflective coating for mid-infrared spectrum. Interestingly, our imprinted antireflective microstructure produced a highly pronounced hydrophobic effect – the first of its type on the surface of chalcogenide glass,

Optics EXPRESS

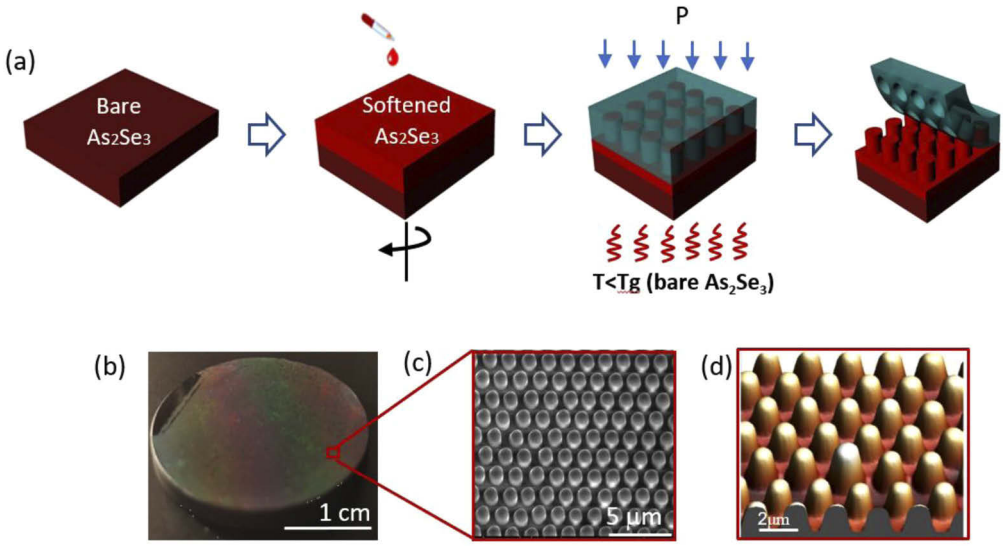

Fig. 1. (a) Direct imprint of chalcogenide glass via surface plasticizing; (a) Schematic process flow, (b) -As_2Se_3 substrate fully imprinted with antireflective and highly hydrophobic moth-eye microstructures, (c) and (d) SEM and AFM of the imprinted microstructures, respectively.

which we characterized by the means of a Cassie–Baxter mechanism. Our novel nanoimprint approach and the demonstrated multifunctional microstructures open the route for the scalable nanoscale surface patterning of chalcogenide glasses, and their numerous applications.

2. Results and discussion

To produce As_2Se_3 substrates, we mixed As and Se inside a quartz ampoule, fused the mixture in a vacuum, quenched in air, and molded the obtained glass to form discs of 25 mm in diameter and 2 mm in thickness. To form surface layers of plasticized As_2Se_3, either on Si substrates or As_2Se_3 substrates, we first ground As_2Se_3 to obtain a fine powder and dissolved the powder in ethylenediamine (EDA). We then applied the obtained solution onto either Si or As_2Se_3 substrates by spin-coating and prebaked the formed film for 2 hour at 80°C. The thickness of the obtained film ranged from 1 to 3 microns, depending on As_2Se_3 concentration and the spinning parameters. The prebaked films were then annealed for 7 hours at different temperatures, to controllably evacuate the excess EDA from the films. Importantly, all the steps were done in an inert atmosphere inside a glove-box, to prevent oxidation of As_2Se_3 and formation of crystalline defects at its surface [29].

Before the direct imprinting of As_2Se_3 films on As_2Se_3 substrates, we had to optimize the imprint parameters, at which the film can be softened by heating above its T_g to be imprinted while keeping the bulk As_2Se_3 substrate below its own T_g to prevent its deformation. Here, we hypothesized that the T_g of the plasticized film depends on the amount of the residual solvent, and thus can be tuned by the annealing conditions. To verify this hypothesis, and establish the process window for our imprint process, we spin-coated As_2Se_3 films on silicon substrates, annealed them at different temperatures, and measured their T_g by nanoindentation. We placed the substrates with the films on a nanoindenter stage with controlled heating and measured the indentation depth using a constant force rate of 1 mN/s until the force reached 10 mN, held the indenter at this force for 5s, and unloaded the indenter with a constant unloading rate of 1 mN/s. An example of a load-indentation curve is given in Fig. 2(a). We repeated the measurements at

Optics EXPRESS

different temperatures for each sample and assessed the T_g in each case, based on the temperature at which the indentation depth increased abruptly (Fig. 2(b)). Figure 2(c) shows the T_g of different samples vs. the annealing temperature of As_2Se_3. As expected, we obtained a general trend by which T_g gradually increases with the annealing temperature. The highest T_g (~175°C) was obtained for the film annealed at 170°C. This T_g is, however, still lower than the T_g of bulk As_2Se_3, which is 185°C [19]. We believe that a higher T_g of solution deposited As_2Se_3 films can be obtained by annealing at a higher temperature and for a longer time, which will cause further removal of EDA and densification of As_2Se_3. Yet, in the context of lithographic imprinting of plasticized As_2Se_3 film, it is desirable to keep the T_g of the film below that of the substrate, and thereby enable thermal imprinting of the film without deforming the substrate. Based on the obtained data, As_2Se_3 film with no annealing, whose T_g is 80°C, or As_2Se_3 annealed at a relatively low temperature, can be imprinted below the glass transition point of bare As_2Se_3, and this completely addresses our requirements. Importantly, all the obtained films were very uniform and with no visible defects, most probably because they were annealed in an inert atmosphere that prevented oxidation and crystallization of As_2Se_3. These results together provide a process window to yield high-quality plasticized As_2Se_3 films with tuned T_g, which, in turn, opens a route for the direct imprinting of bulk As_2Se_3.

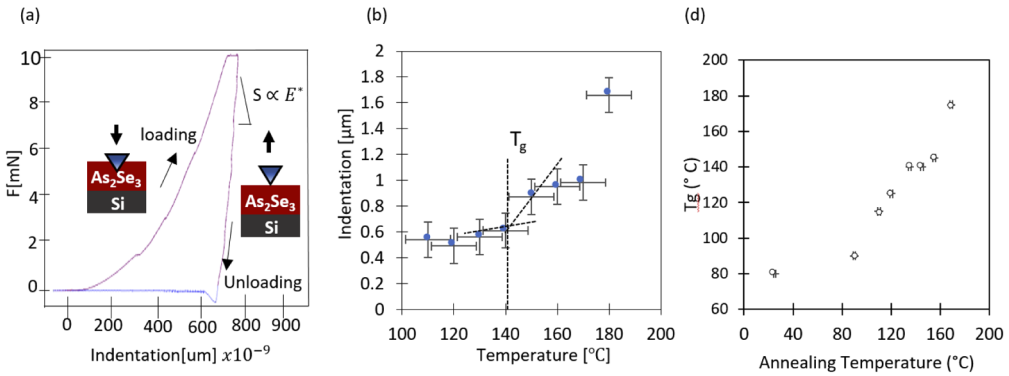

Fig. 2. Determination of glass transition temperature of plasticized As_2Se_3: (a) A typical force-loading curve obtained by nanoindenter. (b) Indentation depth vs. sample temperature for As_2Se_3 annealed at 140°C. (c) T_g of As_2Se_3 vs annealing temperature.

The performance of a functional structure imprinted on the surface of chalcogenide glass depends not only on the shape of the structure geometry but also on the composition and properties of the imprinted material itself. It was previously shown that the solution processing of chalcogenide glasses can largely modulate their composition, structural morphology, and properties [23,29,30]. To ensure that plasticized As_2Se_3 films have a composition and optical properties close to those of pristine As_2Se_3, we performed a series of chemical, structural and optical characterizations. As mentioned above, previous studies on the solution processing of chalcogenide glasses showed their crystallization, which generates optical defects, and produces optical losses [31]. Here, we first verified the absence of macroscopic crystallites using an optical microscope (Fig. S1). Then, we performed a more detailed morphological study using X-ray diffraction (XRD).

Figures 3(a)–3(c) show XRD spectra of bare As_2Se_3, the spin-coated film of As_2Se_3 without annealing, and then spin-coated As_2Se_3 film annealed a 155°C for 7 hours. The three spectra are indicative of a glassy structure. The absence of any narrow peaks in the annealed film in Fig. 3(c) indicates complete amorphousness. In other words, the obtained glass layer lacks any crystallinities that could damage its optical properties. We attribute the absence of crystallinities

Optics EXPRESS

to the fact that all the processing steps were done in an inert atmosphere, which prevents oxidation of As_2Se_3 and, as a consequence, its crystallization [32].

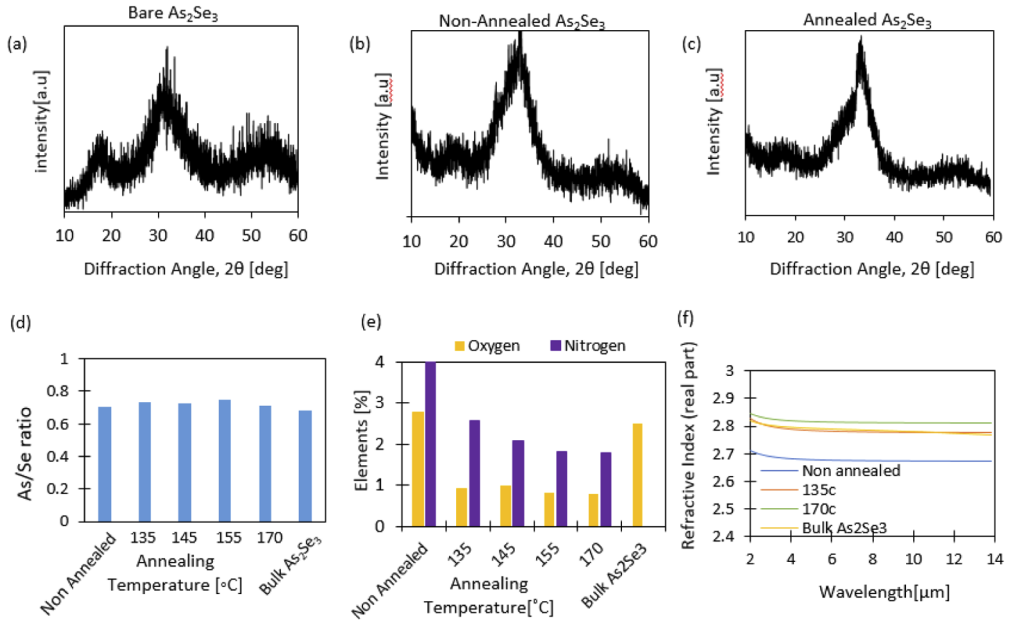

Fig. 3. (a)–(c) XRD spectra of bare (bulk) As_2Se_3, As_2Se_3 layer deposited form solution without annealing, and As_2Se_3 layer deposited from solution and annealed at 170°C, respectively. (d) XPS elementary analysis of As/Se ratio, taken at the depth of 200 nm, (e) EDS analysis of oxygen and nitrogen, (f) refractive index vs. wavelength for bulk As_2Se_3, and plasticized layers with and without annealing.

To verify that plasticized As_2Se_3 films retain the chemical composition of pristine As_2Se_3, we characterized the films using X-ray photoelectron spectroscopy (XPS), focusing on the ratio between As and Se atoms (Fig. 3(d)). Here, we again compared between bulk (i.e pristine) As_2Se_3, the non-annealed film of As_2Se_3, and an As_2Se_3 film annealed at 155°C for 7 hours. We found that As/Se ratio was only slightly changed throughout the processing steps, from 0.71 for the non-annealed film to 0.74 for the film annealed at 170°C. An additional important aspect of the chemical composition of the obtained As_2Se_3 film is the residual solvent, which causes the film plasticizing. EDA contains only carbon, nitrogen, and hydrogen. Hydrogen cannot be detected by XPS. Also, Neither carbon or nitrogen can be quantitatively measured by XPS, because C*-N peak at 286 eV, which is a common surface marker for nitrogen-containing organic molecules overlaps with the Auger peak of Se, and N*-C peak at 400 eV overlaps with the SeLM5 peak. As an alternative to XPS, we used energy dispersive spectroscopy (EDS) to quantify the nitrogen content. Figure 3(e) shows the data for nitrogen and oxygen content in pristine As_2Se_3, and the solution-processed films with and without further annealing at different temperatures. We can see that the non-annealed film contains about 4% of nitrogen, which can be attributed to EDA. However, this value fell to about 1.8% upon annealing at 170°C. Remarkably, for a very low concentration of nitrogen as detected, the dependence of the concentration on the annealing conditions is not obvious. For instance, samples annealed at 155°C and 170°C show similar nitrogen content of about 1.8%, although they have different glass transition temperatures. We believe that there could be a little difference between the samples in terms of the nitrogen content, which is hardly detectable by EDS whose quantification inaccuracy is up to 0.5%. We also believe that the relatively high amount of oxygen in the non-annealed sample originates in water

Optics EXPRESS

and oxygen molecules that have been absorbed in the film when. These molecules are released from the film upon the annealing. Remarkably, EDS analysis of films was done right after their preparation, together with EDS of bulk As_2Se_3 that was prepared a few months in advance. High oxygen content on in the bulk As_2Se_3 can be thus attributed to organic contamination that had been generated on its surface during these months. In general, we see the amount of EDA decreased with annealing temperature, most probably due to its diffusion and evaporation. This gradual decrease in EDA mirrors the previously observed increase in the film T_g with annealing temperature. Overall, controlling the content of EDA, which serves here as a plasticizing agent, is the key to modulate the T_g of As_2Se_3. Remarkably, this modulation which is within the relatively large range of a few tens of degrees is achieved by a very small amount of EDA.

Maintaining the composition of the plasticized film is important for its optical properties, which must be as similar as possible to those of pristine As_2Se_3. We first measured the refractive index of plasticized As_2Se_3 films annealed at different conditions vs. the wavelength within the infrared region, which is most relevant for the optical applications of this material. (Figure 3(f)). The gradual increase in the real part of the refractive index is obviously due to the evaporation of the solvent residuals, and the densification of amorphous As_2Se_3 glass. This trend mirrors previous reports on the effect of annealing conditions on solution-processed As_2Se_3 [29] and As_2S_3 [33,34] films, as well as on thermally evaporated films of chalcogenide glass [35,36]. Notably, the index of As_2Se_3 film annealed at 170°C is slightly higher than that of bulk As_2Se_3 film, probably due to its densification during the long annealing [37].

So far, we have demonstrated the tuning of the T_g of plasticized chalcogenide glass films, while keeping their composition and optical properties similar to that of pristine chalcogenide glass. This enables the production of direct and maskless surface patterning with functional microstructures via soft imprinting. As an example of such fabrication, we imprinted a diffraction grating onto a plasticized surface of As_2Se_3 substrate. For this purpose, we first produced a master mold by photolithography on a Si substrate followed by plasma etching and resist removal. We then replicated the etched structures into hybrid hard-soft PDMS stamp [38], and used it to imprint a plasticized As_3Se_3 film deposited from solution onto a bulk As_2Se_3 substrate and baked at 80°C for two hours in the Nitrogen atmosphere, with no further annealing. We then imprinted As_3Se_3 using a custom-made imprinting tool [27,28,39,40], which is based on conductive heating of the imprinted substrate and anisotropic pneumatic pressure applied onto the attached soft stamps through a flexible membrane (Fig. S2). We used the following imprint parameters: the pressure of 4 bar, time of 20 min, and temperature of 155°C. The value of the imprinting temperature was deliberately chosen between the T_g of non-annealed As_2Se_3 film, previously found to be 135° C and the T_g of bulk As_2Se_3 equal to 185°C. We imprinted two diffraction gratings with periodicities of 10 μm and 20 μm. Figures 4(a) and 4(b) show the 3D and z-section AFM images of the used stamps and their corresponding imprinted structures. It can be seen that the imprinted gratings exactly replicated those of the stamps in terms of periodicity and duty cycle. Furthermore, the obtained depths of the imprinted trenches fit in both cases to the height of the trenches on the stamps, thus indicating that full pattern transfer was achieved upon the used imprinting conditions.

It should be noted that during the imprint, the residual solvent is partially evacuated from the plasticized film and absorbed in the stamp due to the high imprint temperature [40]. In addition, we ensured that the final imprinted structure contains a minimal amount of residual solvent, whilst retaining a composition and optical properties as close as possible to those of pristine material, by annealing the imprinted sample at 155°C for 1 hour in a vacuum. Remarkably, we found that the geometry of the imprinted grating did not change after the annealing. This finding is somehow surprising since we would expect that the evacuation of the solvent during the high-temperature annealing would cause the As_2Se_3 to shrink, and as a result, would lower the imprinted feature height. The fact that no lowering was observed upon annealing indicates

Optics EXPRESS

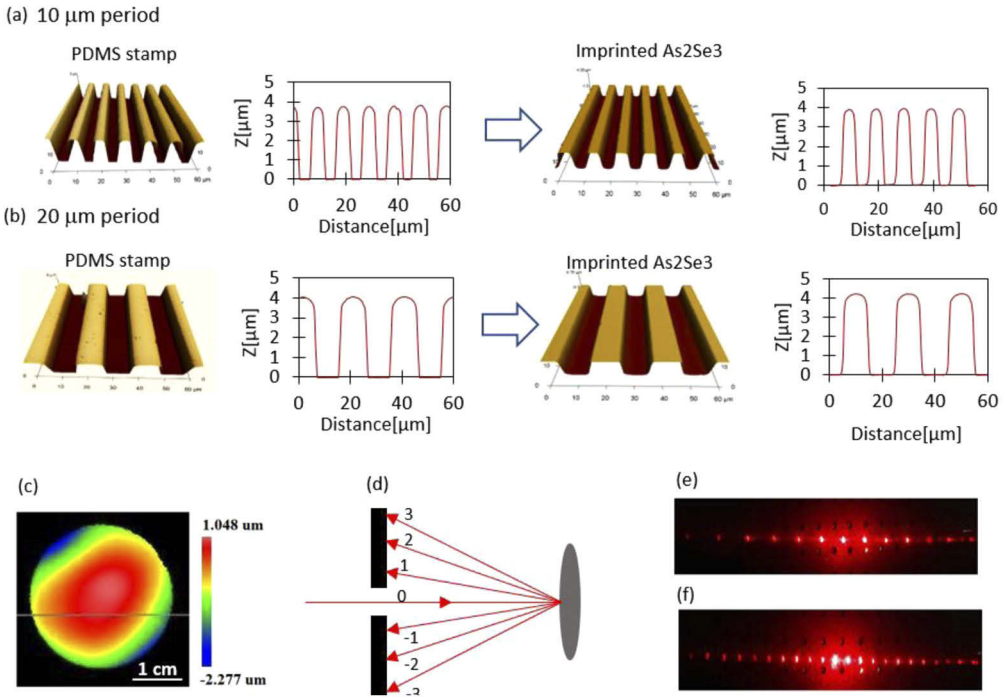

Fig. 4. Diffraction grating directly imprinted on chalcogenide glass: (a) and (b) AFM (3D scanning and x-section plot profile) of PDMS mold and corresponding imprinted pattern for diffraction gratings with 10 μm and 20 μm periods, respectively. (c) 2D laser interferometry scan of the backside of the imprinted As_2Se_3 substrate, showing that the surface was deformed during the imprinting. (d) Scheme of the measurement of diffraction angles. (e) - (f) Diffraction patterns obtained from 10 μm and 20 μm gratings, respectively.

that most of EDA was already evacuated during the imprinting so that the amount of EDA within As_2Se_3 after imprinting was already very low, and its change upon high-temperature annealing was negligible, thus hardly affecting As_2Se_3 volume changes. We, therefore, conclude that the imprint process, whose main purpose was to produce the 3D structures on the As_2Se_3 surface, also produced an annealing effect, which explains why further solvent evacuation during the post-imprint annealing had a negligible influence on feature height.

As mentioned above, while imprinting the surface of a functional material or device, special care must be taken to maintain its original shape, and to prevent its deformation that might be caused by applying excessively high temperature and pressure. In our process, this is ensured by choosing an imprinting temperature below that of the T_g of bulk As_2Se_3. To verify that imprinted As_2Se_3 is not deformed during the imprinting process, we scanned the reverse surface of the imprinted As_2Se_3 substrate using a laser interferometer. The obtained scanning profile (Fig. 4(c)) shows a relatively small bow of $\sim$ 3 microns over the 2.5 cm diameter of the substrate. This bow is similar to that of the original As_2Se_3 substrate before imprint. We conclude therefore that no additional bow was generated during the imprinting. Importantly, a combination of full pattern transfer with no generation of the bow is non-trivial for direct thermal imprinting. Previous reports on the direct imprinting of chalcogenide glasses showed either incomplete pattern transfer [24], or complete pattern transfer with no mention of characterization of bow [25–27]. Recently, we reported full pattern transfer by direct radiative imprinting of As_2Se_3, in which the bow was prevented by supporting the reverse side of the imprinted As_2Se_3 substrate with a flat substrate of

Optics EXPRESS

BK7 glass [28]. Here, we demonstrate a more robust and simpler approach to achieve the same challenging combination of full pattern transfer and non-deformed substrate.

To demonstrate the optical functionality of the imprinted diffraction gratings, we characterized their diffraction angles in reflection mode, using a HeNe laser (λ=632.8 nm). The setup is schematically shown in Fig. 4(d), and the angles were calculated based on the distances between the spots in the diffraction pattern formed on a black board (Fig. 4(e)). The obtained angles (Table 1) perfectly match those calculated from the grating period using Bragg's law ($\sin\theta=n\lambda/p$). These results are an additional confirmation of the high pattern fidelity of our imprinting process.

Table 1. Calculated and measured diffraction angles of the imprinted gratings.

Periodicity	Diffraction order	±1	±2	±3	±4
10 μm	Calculated angle	3.6°	7.7°	10.5°	14.4°
	Measured angle	3.6°	7.3°	10.9°	14.7°
20 μm	Calculated angle	1.6°	3.6°	5.7°	7.3°
	Measured angle	1.8°	3.6°	5.4°	7.3°

So far, we have demonstrated the direct imprinting of chalcogenide glass with features sized on the micron scale. However, imprinting of much smaller features, sized down to the sub-micron scale, is often required for some optical applications, such as high-performance wave-guides for near IR [30]. To explore the resolution limits of our nanoimprint approach, we produced a master mold with a series of patterns of sub-100 nm feature size using electron-beam lithography. We then replicated a soft stamp from this master mold and used it for direct thermal imprinting of As_2Se_3. Figure 5(a) presents a typical 2D grating with 200 nm periodicity. Here, the exact width of the imprinted line was estimated from full-width half maximum (FWHM) of the cross-section profile of the high-resolution greyscale image of the imprinted lines (Fig. 5(a) inset), and it was found to be equal to 20 nm (Fig. 5(b)), which precisely mirrored the linewidth in the electron-beam patterned mold. SEM images also show negligible line-edge roughness (LER), which most probably stems from the LER of the master mold. The ultra-small size of the imprinted features as well as their low LER confirm that plasticized chalcogenide glasses are greatly suitable for high-quality and high-resolution pattern transfer by direct imprinting.

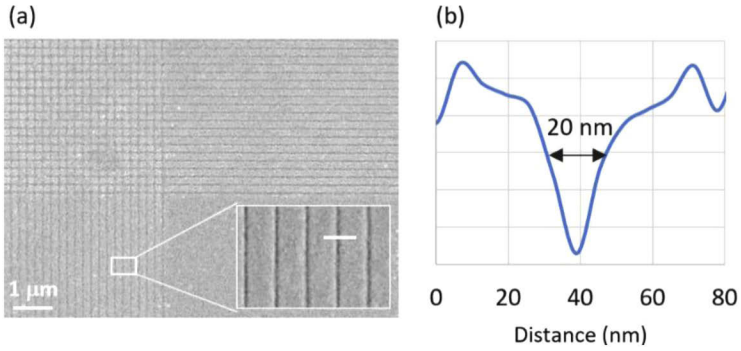

Fig. 5. (a) Imprinted pattern of 2D grating with 200 nm period and 20nm line width. (b) Cross-section SEM color profile of the imprinted line in the inset of Fig. 5(a), with the measured FWHM.

Additionally, an important application of direct imprinting we explored is the fabrication of antireflective microstructures. We produced antireflective structures of periodic bumps with a periodicity of 2 μm, a duty cycle of 0.75, and a height of 1.4 μm, to provide an optimal reduction

Optics EXPRESS

in surface reflection for a wavelength range of 8–13 μm. For this purpose, we first produced a master mold by self-assembly of 2 μm polystyrene microspheres on a silicon substrate, followed by trimming of the microspheres in an oxygen plasma, and etching the underlying Si through the mask formed by the microspheres (Fig. S3). Here, the diameter of the microspheres defined the periodicity of the moth-eye structure, and the trimming time was used to control the duty cycle. We then replicated a PDMS stamp from the Si master mold and used it to imprint an As_2Se_3 substrate coated with a plasticized As_2Se_3 film, by the protocol described above. Figure 6(a) shows 3D and z-section AFM of the PDMS stamp and of the imprinted As_2Se_3 moth-eye structure, for both tested geometries of the diffraction grating, and Fig. 6(b) shows SEM of the imprinted structure. Again, the shape and height of the imprinted structures, when compared to those of the stamp, indicate full pattern transfer with very high pattern fidelity, which can be further confirmed by SEM images of the imprinted As_2Se_3 surface.

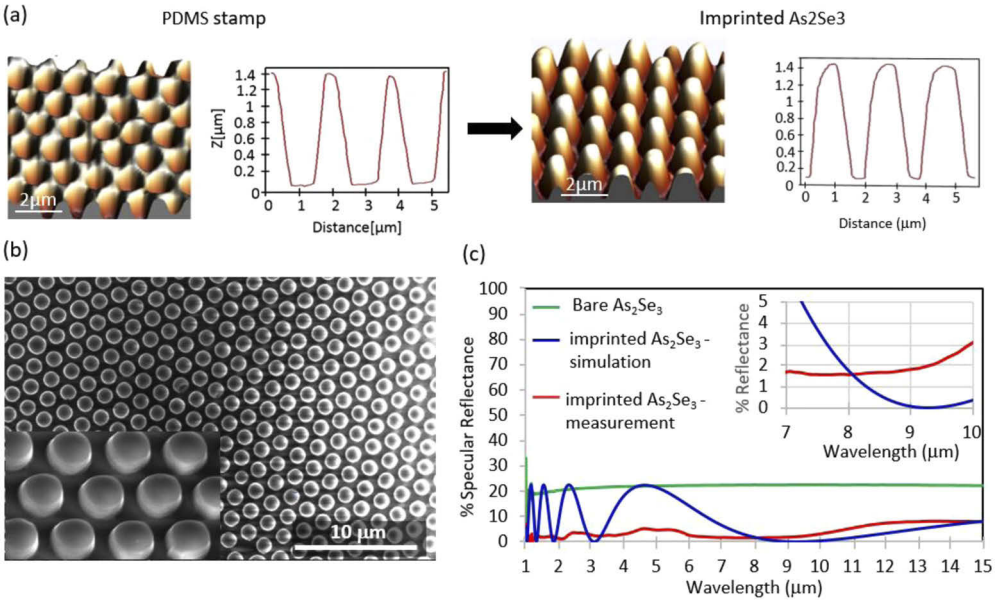

Fig. 6. Antireflective structure directly imprinted on As_2Se_3. (a) AFM of the soft mold used to imprint the structure, and its pattern transferred to the As_2Se_3 surface. (b) SEM of the imprinted antireflective structure. Inset shows high magnification tilted SEM. (c) The reflectance spectrum of surface imprinted with antireflective (red), compared to that of bare As_2Se_3 surface (green), and a simulated spectrum (blue). The inset shows the simulated and measured spectra in the range of 7–13 μm.

The specular reflectance spectrum of the surface imprinted with antireflective structures, as compared to that of bare As_2Se_3 surface, is shown in Fig. 6(c). Importantly, the reverse side of measured substrates was ground before the measurements, to minimize the effect of backside reflection. The measured spectrum is also compared to the simulated spectrum, which was calculated for a single layer antireflective coating, whose thickness is equal to the height of the antireflective microstructures, and whose effective refractive index is calculated as the sum of the As_2Se_3 and air indices multiplied by their volume fractions within the antireflective structure. From the comparison, it is seen that the imprinted antireflective structure produces a very low reflection in the desired wavelength range of 8–10 μm (shown in inset), with, however, a flattened minimum, which is shifted toward lower wavelengths. This indicates that the imprinted antireflective structures have a certain height distribution, which might stem from variations in

Optics EXPRESS

the depth of plasma-etched features in the mold used to prepare the imprinting stamp. Also, the simulated spectrum has pronounced interference peaks at lower wavelengths, which are absent in the measured spectrum. This absence in the case of the measured spectrum is due to the dominance of optical scatterings at this wavelength range, which are not taken into account in the used simulation. However, the small peaks of the second diffraction order at ~ 4.5 μm and third diffraction order at ~2.4 μm are similar for both simulated and measured spectra. Notably, the measured data represents the specular reflectance, which does not include the effects of solid diffraction angles and scattering. However, these effects are negligible for the range of 8-13 microns, with the range of interest for our antireflective design.

Besides the attractive antireflective properties, microstructured surfaces possess fascinating hydrophobic properties, which are also bioinspired [41], and are often termed as "lotus leave effect". This effect is particularly important for optical applications due to its self-cleaning potential: microstructures that repel water prevent surface contamination and thus contribute to the long-term reliability and high performance of optical components. For this reason, patterned microstructures have often been produced for two purposes – antireflection and water-repellent – using various bottom-up and top-down fabrication approaches applied to common optical materials such as silica glass [15]. However, hydrophobic microstructures on chalcogenide glasses have not been demonstrated up to date, to the best of our knowledge. Here, we used the directly imprinted moth-eye microstructures described above as a highly hydrophobic coating on As_2Se_3. We characterized the wetting properties of imprinted chalcogenide glass by measuring advancing contact angle (θ) of water-ethanol mixtures at different ratios, and compared these to the angles on pristine flat As_2Se_3 (Fig. 7(a)). Interestingly, for most of the water-ethanol ratios, the advancing contact angle on the patterned surface was only slightly higher than that on the flat surface. However, the contact angle of pure water on the micropatterned surface was 150°, compared to 95° on the bare surface, indicating a pronounced highly hydrophobic behavior of the imprinted moth-eye pattern. To confirm that the observed high hydrophobicity stems from the lotus leaf effect produced by the imprinted microstructures, we plotted $cos\theta$ of the patterned surface vs. $cos\theta$ of the non-patterned surfaces (Fig. 7(b)), to obtain a wetting diagram [42]. Here, the majority of the points lay close to the diagonal of the upper-right corner of the plot, reflecting

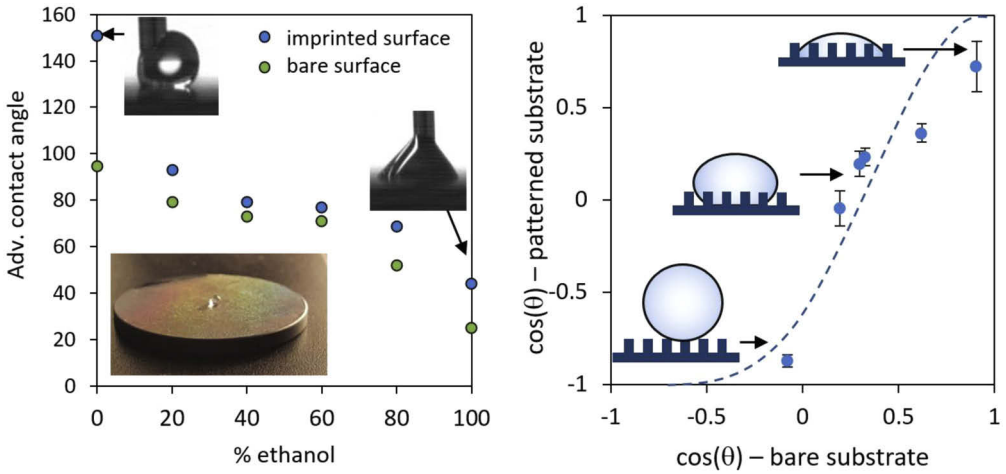

Fig. 7. Wetting properties of the imprinted As_2Se_3 surface. (a) Advancing contact angles of water-ethanol mixture for imprinted and bare surfaces. Inset shows a photograph of an imprinted As_2Se_3 substrate with a water drop (c) Wetting diagram indicating the transition between different wetting states of the imprinted surface.

Optics EXPRESS

similar values of contact angle for both surface types. These points represent the Wenzel state, for which the liquid wets the microstructure surface completely. An exceptional point at the bottom of the plot represents Cassie-Baxter state, at which air pockets are trapped between the imprinted structures, resulting in incomplete surface wetting, and substantially higher wetting angle compared to that obtained on the flat surface.

3. Experimental setup

3.1. Preparation of plasticized As_2Se_3 layer

Bulk As_2Se_3 chalcogenide glass was ground into a powder and mixed with EDA in a 2:3 mass ratio. The mixture was stirred at 80°C for 12 hours until complete dissolution. After transfer to a glove box with a nitrogen atmosphere. The solution was spin-coated either on Si or As_2Se_3 substrates, followed by soft baking at 80°c for 2 hours. Spinning at 1000 rpm for 15 s produced a film thickness of ~2.5 μm.

3.2. Compositional, structural and mechanical characterizations of plasticized As_2Se_3 layer

XRD spectra were was measured using Rigaku Spectrometer, D/max-2100, Cu(kα) source, Pass energy of 40 keV. XPS data were collected using an X-ray photoelectron spectrometer ESCALAB 250 ultrahigh vacuum (1×10^{-9} bar) apparatus with an Al(K^{α})X-ray source and a monochromator. X-ray beam size was 500 μm and survey spectra were recorded with pass energy (PE) 150 eV and high energy resolution spectra were recorded with pass energy (PE) 20 eV. To correct for charging effects, all spectra were calibrated relative to a carbon C 1s peak positioned at 284.8 eV. Processing of the XPS results was carried out using AVANTAGE software. As3d and Se3d peaks were evaluated at 42.75 eV and 54.85 eV, respectively. EDS measurements were performed using a scanning electron microscope fitted with EDS detector with 15kV for 1μm depth. A nano-indenter (MFP, Asylum Research) was used for T_g measurement of the annealed thin layers. For each measurement, the samples were heated up in 10°C steps, from 130 to 170°C. The indentation was carried out under a constant load of 10 mN for 5 seconds. Force indentation curves were plotted for each measurement.

3.3. Optical measurement of As_2Se_3 plasticized layers

The refractive index of the As_2Se_3 plasticized layers was measured using a Woollam IR VASE spectroscopic ellipsometer. Data were collected in the 2-40 μm range. The fitting was performed using the WVASE software. The As_2Se_3 film was assumed to be isotropic, and a non-absorbing Cauchy model was fitted in the 2-13 μm range. The reflection measurements of the As_2Se_3 films were obtained using a Perkin Elmer Frontier optics FTIR spectrometer using an 8° reflection accessory and a Ge wedge for reference. Reflection spectra of the antireflection subwavelength structures were simulated used the OPTILAYER thin film software.

3.4. Fabrication of imprint stamps

First, masters for the stamp cast were prepared. For the diffraction grating, the master was prepared using photolithography of Az2020 negative resist on silicon substrate, followed by electron-beam evaporation of Ni (100 nm), lift-off in hot acetone, Si dry etching in SF_6/C_4F_8 plasma (36sccm SF6, 15sccm C2H4, RF=15W, LF=250W, 25min) though the Nickel mask, and Nickel strip using piranha (H_2SO_4/H_2O_2 1/3) solution. The master with antireflective and highly hydrophobic pattern was prepared by colloidal lithography using polystyrene microspheres of 2μm diameter in a Langmuir-Blodgett trough. Then, the microsphere diameter was reduced to 1.5 μm by dry etching in O_2 plasma (100sccm O_2, RF=15_W, LF=200_W, 30sec). The microsphere pattern was transferred to Si by dry etching as described above, and the remaining microspheres

Optics EXPRESS

were removed by sonication in hot chlorobenzene. The master mold with nanometric features was fabricated by electron beam lithography (Raith eLine) using PMMA as a positive resist. No pattern transfer to Si was done in this case, and patterned PMMA was directly used for the replication of the soft stamp. Hybrid soft stamps were replicated from the fabricated masters using previously reported protocol [38].

3.5. Direct thermal imprinting

The imprint was done in a custom-built tool (Fig. S1). A plasticized As_2Se_3 surface was first brought in contact with a soft stamp, the two were then placed between two silicone elastomeric membranes, and positioned onto the heating plate inside the pressure chamber. The chamber was vacuumed to prevent the formation of air bubbles and the subsequent oxidation of the imprinted surface. Then, the substrate was heated to 155°C, and a pressure of 4 bars was applied for 20 minutes, followed by gradual cooling at room temperature. The imprinted patterns were characterized by SEM and AFM. The flatness of the imprinted substrate was characterized by ZYGO Verifire (λ=0.63μm).

4. Conclusion

In summary, we introduced a highly versatile approach for the surface nano-patterning of chalcogenide glasses. The main feature of this approach is its unique combination of full pattern transfer whilst maintaining the original substrate shape. Another remarkable feature of our approach is in its ability to produce 3D surface structures with arbitrary geometries using "resistless" patterning, e.g. without application of foreign material such as lithographic resist, and with no need for post-lithographic pattern transfer by etching. Tuning of thermo-mechanical properties of chalcogenide glass, e.g. T_g and elastic modulus, by its plasticizing with a commonly used solvent and without changing its optical properties, opens an intriguing route to numerous processing methods. In this work, we focused on As_2Se_3 plasticized by EDA. On the other hand, EDA, as well as similar solvents such as propylene-diamine, can dissolve other chalcogenide glasses such as As_2S_3, $As_xS_ySe_{1-x-y}$, and $Ge_xSb_yS_{1-x-y}$ [43]. Thus, our fabrication approach can be generalized to numerous combinations of chalcogenide glasses and solvents. Also, in this work, we explored only one processing method – surface micropatterning. However, plasticizing chalcogenide glasses can, in principle, facilitate other thermoforming processes, such as molding, and these processes should be explored in the future. We demonstrated the effective fabrication of sub-wavelength antireflective microstructures that also have water-repelling properties. This combination, which has been previously explored for common optical materials, but is unprecedented for chalcogenide glasses, opens a pathway to numerous applications of these important optical materials.

Funding

PAZY Foundation.

Disclosures

The authors declare that there are no conflicts of interest related to this article.

References

1. A. Zakery and S. R. Elliott, "Optical properties and applications of chalcogenide glasses: A review," J. Non-Cryst. Solids **330**(1-3), 1–12 (2003).
2. C. R. Petersen, "Mid-infrared supercontinuum covering the 1.4–13.3 μm molecular fingerprint region using ultra-high NA chalcogenide step-index fibre," Nat. Photonics **8**(11), 830–834 (2014).
3. H. Lin, "Chalcogenide glass-on-graphene photonics," Nat. Photonics **11**(12), 798–805 (2017).

Optics EXPRESS

4. A. Zakery and S. R. Elliott, "Optical nonlinearities in chalcogenide glasses and their applications," *Springer Ser. Opt. Sci.* 135, 1–28 (2007).
5. K. Tanaka, "Structural phase transitions in chalcogenide glasses," Phys. Rev. B **39**(2), 1270–1279 (1989).
6. M. Wuttig, H. Bhaskaran, and T. Taubner, "Phase-change materials for non-volatile photonic applications," Nat. Photonics **11**(8), 465–476 (2017).
7. J. Q. Xi, "Optical thin-film materials with low refractive index for broadband elimination of Fresnel reflection," Nat. Photonics **1**(3), 176–179 (2007).
8. S. Shabahang, "Robust multimaterial chalcogenide fibers produced by a hybrid fiber-fabrication process," Opt. Mater. Express **7**(7), 2336 (2017).
9. E. Brinley, S. Seal, R. Folks, E. Braunstein, L. Kramer, and S. Seal, "High efficiency SiO2–TiO2 hybrid sol-gel antireflective coating for infrared applications," J. Vac. Sci. Technol., A **24**(4), 1141–1146 (2006).
10. C. G. Bernhard and W. H. Miller, "A Corneal Nipple Pattern in Insect Compound Eyes," Acta Physiol. Scand. **56**(3-4), 385–386 (1962).
11. Y. F. Huang, "Improved broadband and quasi-omnidirectional anti-reflection properties with biomimetic silicon nanostructures," Nat. Nanotechnol. **2**(12), 770–774 (2007).
12. W.-L. Min, B. Jiang, and P. Jiang, "Bioinspired Self-Cleaning Antireflection Coatings," Adv. Mater. **20**(20), 3914–3918 (2008).
13. S. Y. Heo, "Bifunctional Moth-Eye Nanopatterned Dye-Sensitized Solar Cells: Light-Harvesting and Self-Cleaning Effects," Adv. Energy Mater. **4**(3), 1300632 (2014).
14. X. Li, J. He, and W. Liu, "Broadband anti-reflective and water-repellent coatings on glass substrates for self-cleaning photovoltaic cells," Mater. Res. Bull. **48**(7), 2522–2528 (2013).
15. K. C. Park, H. J. Choi, C. H. Chang, R. E. Cohen, G. H. McKinley, and G. Barbastathis, "Nanotextured silica surfaces with robust superhydrophobicity and omnidirectional broadband supertransmissivity," ACS Nano **6**(5), 3789–3799 (2012).
16. S. Schroeter, M. Vlček, R. Poehlmann, and A. Fišerová, "Efficient diffractive optical elements in chalcogenide glass layers fabricated by direct DUV laser writing," J. Phys. Chem. Solids **68**(5-6), 916–919 (2007).
17. J. Wei and X. Jiao, "Super-resolution nanopatterns and optical recording in chalcogenide phase change thin films by direct laser writing," in *Proceedings of SPIE - The International Society for Optical Engineering*, 2009.
18. A. Zoubir, "Direct femtosecond laser writing of waveguides in As2S3 thin films," Opt. Lett. **29**(7), 748–750 (2004).
19. V. S. Shiryaev and M. F. Churbanov, "Preparation of high-purity chalcogenide glasses," in *Chalcogenide Glasses*, 2013.
20. T. Han, S. Madden, D. Bulla, and B. Luther-Davies, "Low loss Chalcogenide glass waveguides by thermal nano-imprint lithography," Opt. Express **18**(18), 19286 (2010).
21. M. Solmaz, H. Park, C. K. Madsen, and X. Cheng, "Patterning chalcogenide glass by direct resist-free thermal nanoimprint," J. Vac. Sci. Technol., B **26**(2), 606–610 (2008).
22. S. Danto, "No Title," *Proc. SPIE*, vol. 9884, pp. 88841T–1, 2013.
23. Y. Zou, "High-Performance, High-Index-Contrast Chalcogenide Glass Photonics on Silicon and Unconventional Non-planar Substrates," Adv. Opt. Mater. **2**(5), 478–486 (2014).
24. J. Orava, T. Kohoutek, L. Greer, and H. Fudouzi, "Soft imprint lithography of a bulk chalcogenide glass," Opt. Mater. Express **1**(5), 796–802 (2011).
25. M. R. Lotz, C. R. Petersen, C. Markos, O. Bang, M. H. Jakobsen, and R. Taboryski, "Direct nanoimprinting of moth-eye structures in chalcogenide glass for broadband antireflection in the mid-infrared," Optica **5**(5), 557–563 (2018).
26. M. Lotz, J. Needham, M. H. Jakobsen, and R. Taboryski, "Nanoimprinting reflow modified moth-eye structures in chalcogenide glass for enhanced broadband antireflection in the mid-infrared," Opt. Lett. **44**(17), 4383 (2019).
27. D. Yehuda, E. Kassis, S. Joseph, and M. Schvartzman, "Direct soft imprint of chalcogenide glasses," J. Vac. Sci. Technol., B **36**(3), 031602 (2018).
28. N. Ostrovsky, D. Yehuda, S. Tzadka, E. Kassis, S. Joseph, and M. Schvartzman, "Direct Imprint of Optical Functionalities on Free-Form Chalcogenide Glasses," Adv. Opt. Mater. **7**(19), 1900652 (2019).
29. Y. Zou, "Effect of annealing conditions on the physio-chemical properties of spin-coated As_2Se_3 chalcogenide glass films," Opt. Mater. Express **2**(12), 1723 (2012).
30. Y. Zou, "Demonstration of high-performance, sub-micron chalcogenide glass photonic devices by thermal nanoimprint," in Integrated Optics: Devices, Materials, and Technologies XVIII, 2014, vol. 8988, p. 898806.
31. C. Tsay, Y. Zha, and C. B. Arnold, "Solution-processed chalcogenide glass for integrated single-mode mid-infrared waveguides," Opt. Express **18**(25), 26744 (2010).
32. P. Sachan, R. Singh, P. K. Dwivedi, and A. Sharma, "Infrared microlenses and gratings of chalcogenide: Confined self-organization in solution processed thin liquid films," RSC Adv. **8**(49), 27946–27955 (2018).
33. T. V Hakkarainen, A. Schramm, J. Mäkelä, P. Laukkanen, and M. Guina, "Lithography-free oxide patterns as templates for self-catalyzed growth of highly uniform GaAs nanowires on Si(111)," Nanotechnology **26**(27), 275301 (2015).
34. S. Song, J. Dua, and C. B. Arnold, "Influence of annealing conditions on the optical and structural properties of spin-coated As 2 S 3 chalcogenide glass thin films," Opt. Express **18**(6), 5472 (2010).

Optics EXPRESS

35. R. P. Wang, S. J. Madden, C. J. Zha, A. V. Rode, and B. Luther-Davies, "Annealing induced phase transformations in amorphous As2S 3 films," J. Appl. Phys. **100**(6), 063524 (2006).
36. N. Carlie, "Measurement of the refractive index dispersion of As 2 Se 3 bulk glass and thin films prior to and after laser irradiation and annealing using prism coupling in the near- and mid-infrared spectral range," Rev. Sci. Instrum. **82**(5), 053103 (2011).
37. B. Gleason, P. Wachtel, J. D. Musgraves, A. Qiao, N. Anheier, and K. Richardson, "Compositional-tailoring of optical properties in IR transparent chalcogenide glasses for precision glass molding," in *Optifab 2013*, 2013, vol. 8884, p. 888417.
38. T. W. Odom, J. C. Love, D. B. Wolfe, K. E. Paul, and G. M. Whitesides, "Improved pattern transfer in soft lithography using composite stamps," Langmuir **18**(13), 5314–5320 (2002).
39. A. Pandey, S. Tzadka, D. Yehuda, and M. Schvartzman, "Soft thermal nanoimprint with a 10 nm feature size," Soft Matter **15**(13), 2897–2904 (2019).
40. M. Rosenberg and M. Schvartzman, "Direct Resistless Soft Nanopatterning of Freeform Surfaces," ACS Appl. Mater. Interfaces **11**(46), 43494–43499 (2019).
41. D. Quéré, "Wetting and Roughness," Annu. Rev. Mater. Res. **38**(1), 71–99 (2008).
42. T. Onda, S. Shibuichi, N. Satoh, and K. Tsujii, "Super-water-repellent fractal surfaces," Langmuir **12**(9), 2125–2127 (1996).
43. Y. Zha, M. Waldmann, and C. B. Arnold, "A review on solution processing of chalcogenide glasses for optical components," Opt. Mater. Express **3**(9), 1259 (2013).